JETIR.ORG ISSN: 2349-5162 | ESTD Year : 2014 | Monthly Issue
JOURNAL OF EMERGING TECHNOLOGIES AND INNOVATIVE RESEARCH (JETIR)
An International Scholarly Open Access, Peer-reviewed, Refereed Journal

# Supercapacitive properties of PANI-$Co(OH)_2$ nanocomposite electrodes

Janardhan H. Shendkar

S. S. J. E. S. Arts, Commerce & Science College, Gangakhed, Dist. Parbhani, India

**Abstract**

I attempt to exhibit comprehensive analysis of experimentally acquired supercapacitive performance of cobalt hydroxide ($Co(OH)_2$)-polyaniline (PANI) hybrid nanocomposites (HNs), prepared potentiostatically via electrochemical deposition method. Morphologically both amorphous electrodes HNs are different from one another. The electrochemical properties of the HNs electrodes have been investigated by cyclic voltammograms measurement. The specific capacitances HNs are found to be 81.63F/g and 142.8F/g respectively, at a sweep rate of 10 mV/s in 1.0 M NaOH electrolyte, whereas the stabilities at a scan rate of 40mV/s assigned to these electrodes, are 39.49% (after 600 cycles) & 82.98% (after 1000 cycles) respectively. My work demonstrates synergetic effect of supercapacitive performance in hybrid/composite nanostructured electrodes.

*Keywords*
Electrochemical Supercapacitors, Nanocomposite, Polyaniline, Specific capacitance, nanostructures, cobalt hydroxide, electrodeposition

## 1 Introduction

Batteries, traditional capacitors and electrochemical supercapacitors (ESs) are electrochemical energy storage and conversion devices, where batteries display lower power and higher energy density, while traditional capacitors demonstrate higher power and lower energy density [1]. Therefore, ESs exhibiting higher power density as compared to batteries and low power density than traditional capacitors, higher energy density than the traditional capacitors and low energy density than batteries, act as a bridge between batteries and traditional capacitors [2]. These devices are being attracting considerable attention in compatible as well as in commercial electrochemical devices [3]. Based on an energy storage mechanism; ES are of two categories *viz.* electrical double layer capacitors (EDLCs) and pseudocapacitors. In EDLCs, the electric charge in the form of electrons, holes and/or ions accumulation occurs at the interface between the surface of electrode and the electrolyte. EDLCs provide relatively higher power due to larger potential

window and excellent cyclability [4]. However, in a pseudocapacitor, the fast and reversible Faradaic reaction at the accessible surface of the electrode by electrolyte establishes its energy storage capability [5]. Typically, the SC of a pseudocapacitor electrode is better than that of an electrode working as an EDLC [6]. Therefore, pseudocapacitors are generally preferred in applications where high capacitance is desired. Polyaniline (PANI) is one the most employed and studied conducting polymers among other conducting polymers from last four decades due to its low-cost, easy synthesis methods, splendid environmental stability, and emulous redox reversibility by both charge transfer doping and protonation [7-9]. By growing a hybrid nanocomposite of PANI with other electrochemically active materials, it is accomplishable to improve the performance of PANI not only by the effect of the size confinement but also by adding functionalities or synergistic properties [4]. The hybrid nanocomposite of PANI with activated carbon, carbon nanotubes, ordered mesopours carbon, carbonization of the PANI nanowires, three-dimensional graphene, $MnO_2$, $WO_3$, $V_2O_5$ and graphene/$Fe_2O_3$ [10 - 18] etc., have demonstrated a strong synergic effect in literature due to which the electrochemical performance of composite in neutral and/or alkaline medium has been considerably boosted.

In this work, the hybrid nano-structured (HN) film electrode was prepared by electrodeposition of $Co(OH)_2$ onto already PANI deposited onto stainless steel substrate.

## 2 Experimental section

### *2.1 Chemicals*

All the chemicals used in present work are analytical reagent grade of Merck. Aniline monomer (99% pure), sulfuric acid ($H_2SO_4$), cobalt nitrate hexahydrated (99% pure), sodium hydroxide, acetone & distilled water are used as purchased without any further purification.

### *2.2 Preparation of PANI electrode*

Polymerization of aniline has been conducted in a one compartment glass cell at room temperature (27°C) using three-electrode potentiostatical approach, controlled by computer. In three-electrode potentiostat, platinum plate of area 1.5 cm x 1.5 cm, Ag/AgCl electrode & stainless-steel (SS) substrate of area 1 cm x 4 cm (for electrodeposition area is 1cm x 1cm ) are used as a counter, reference and working electrodes, respectively. The substrate was ultrasonically cleaned in acetone solution first and then in distilled water for 10 minutes, and then dried by air. The aniline monomer solution of 0.5M is prepared in distilled water by stirring for 5 minutes due to low solubility of aniline in water. The 0.5 M solution of sulfuric acid is poured drop-by-drop slowly in 0.5M aniline solution in order to avoid chemical polymerization to adjust the solution $_P{}^H < 2$. The low $_P{}^H$ value of prepared solution not only allows more amount of deposition of PANI electrode material but also gets the required nanofiber morphology. The solution is further stirred for 5 minutes to obtain well mixed homogeneous solution. This 20 ml homogeneous solution of aniline + sulfuric acid is poured in one compartment glass cell and the platinum plate electrode and SS substrate electrode are immersed parallel to each other to deep 1 cm in solution and 1 cm apart. The Ag/AgCl electrode is dipped in solution at a distance of 1cm apart from both counter and

working electrode. PANI films electrodeposited (anodized) at fixed potential of +0.75 V on 1cm$^2$ surface area of SS substrate *vs.* Ag/AgCl electrode for 5 minutes and is dried for 2 minutes before further use.

*2.3 Preparation of PANI + Co(OH)$_2$ HN*

A 0.05 M aqueous solution of cobalt nitrate hexahydrated is prepared and electrodeposition (cathodization) of Co(OH)$_2$ has been conducted in the one compartment glass cell at room temperature using three electrodes Potentiostat, same as like earlier. The Co(OH)$_2$ electrodes are electrodeposited (cathodized) at fixed potential of -1.0V on previously electrodeposited PANI film (deposited on SS as substrate) *vs.* Ag/AgCl electrode for time intervals of 5 minutes (A) and 15 minutes (B). These HN electrodes are dried at room temperature and immersed in distilled water for 2 minutes to remove impurities. These electrodes are again dried in atmospheric air at room temperature.

*2.4 Characterization details*

The morphologies and elemental analyses of the electrode materials are investigated by a Hitachi S-4800 field-emission scanning electron microscope (FE-SEM). The X-ray diffraction (XRD) measurements were accomplished by using a (Ultima IV, Rigaku 2500) diffractometer with a Cu− Kα radiation in the 2$\theta$ angle range of 10−80°. The electrochemical deposition and the cyclic-voltammetry (CV) of the HN film electrodes are monitored through a WonAtech (WPG 100 Potentiostat / Galvanostat Workstation). All the electrochemical properties were studied in 1.0M NaOH electrolyte solution.

**3 Results and Discussion**

*3.1 Reaction kinetics*

The PANI film prepared from an electrochemical oxidation of the 0.5M aniline monomer and 0.5M sulfuric acid as dopant in a three electrode single glass cell with a constant potential of 0.75V for 5 minutes is used. The electrochemical oxidative polymerization of the aniline monomer inherently forms bluish film of PANI. The Co(OH)$_2$ is cathodically deposited on PANI electrode to produce HNs in 0.05M Co(NO$_3$)$_2$ by reduction of the $NO_3^-$ ions as [19]

$$NO_3^- + H_2O + 2e^- \rightarrow NO_2^- + 2OH^-$$

$$Co^{2+} + 2OH^- \rightarrow Co(OH)_2$$

The $OH^-$ ions formed in the vicinity of cathode surface due to reduction of $NO_3^-$ ions combine with $Co^{2+}$ ions, resulting in the deposition of Co(OH)$_2$ materials on the PANI cathode electrode.

*3.2 Structural elucidation and compositional analyses*

The XRD spectra of the hybrid nanocomposite PANI and Co(OH)$_2$ electrodes are shown in Fig. 1. Peaks marked with * in all XRD patterns are of SS substrate. Thus, PANI electrode is in amorphous nature showing presence of short rang order of benzenoid and quinonoid structural units in the back bone of PANI electrodes. The crystalline structure of PANI is observed only when PANI is in its polaron and/or bipolarons state due to protonation of PANI by protonic acid.

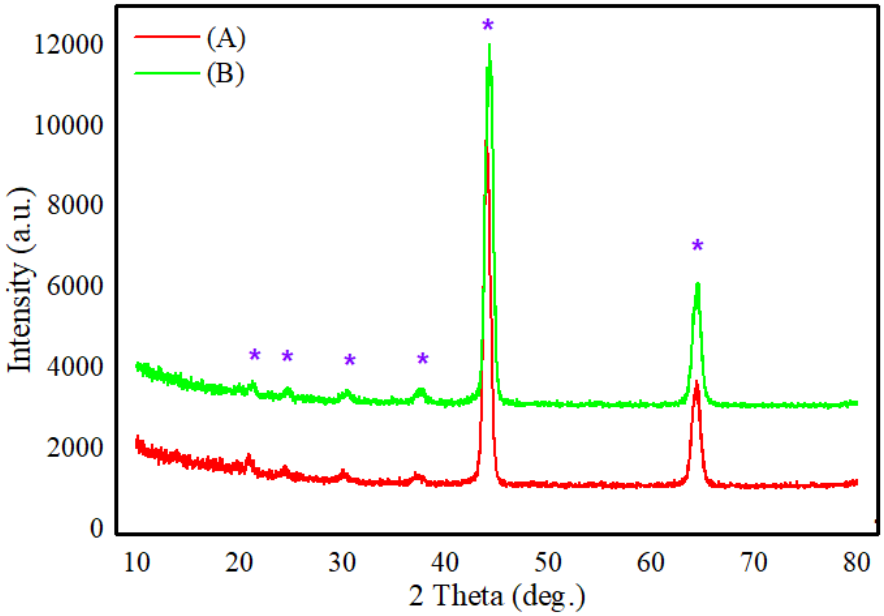


Fig. 1 The XRD patters of HNs (A) and (B) electrodes.

But in the present study, it is immersed in distil water to remove the dopant acid used at the time of polymerization. PANI is reduced at the time of (cathodization at -1.0V) electrodeposition of the $Co(OH)_2$ on it and hence PANI in emeraldine base gets converted into leucoemeraldine base, which generally is amorphous in nature. The $Co(OH)_2$ is also showing amorphous nature, as i) the required time for arrangement of $OH^-$ ions with respect to $Co^{2+}$ ions is low on account of applied negative voltage, and ii) low availability of $OH^-$ ions due to more time required for reduction of $NO_3^-$ ions as compared in formation of $Co^{2+}$ ions at cathode. In the present work, the conventional method of structure determination i.e. XRD pattern cannot be used to predict the presence of elements HNs due to amorphous nature of as-developed electrodes.

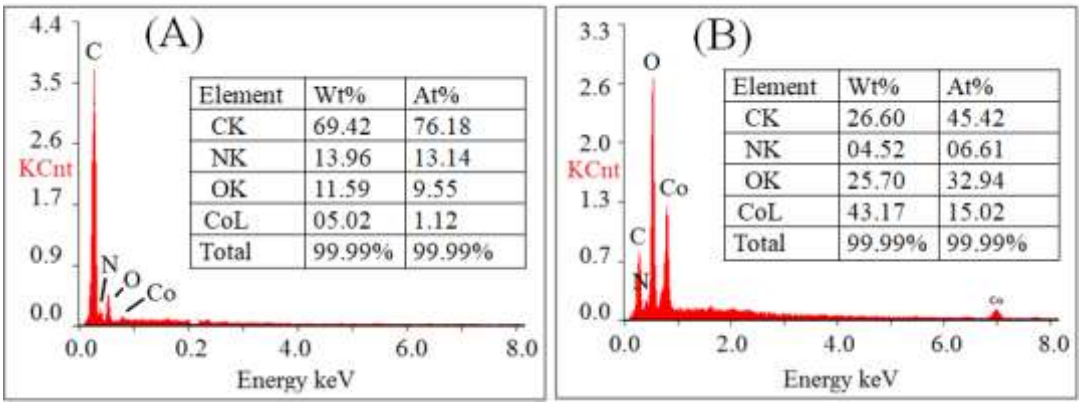


Fig. 2 The EDX mapping on HNs; (A) and (B) electrode surfaces.

From energy dispersive X-ray (EDX) spectrums [Fig. 2], the plots of the energy in keV versus relative kilo counts of the detected X-rays from electrode material, carbon, C, peak at 0.24 keV, nitrogen, N, peak at 0.35 keV, oxygen, O, peak at 0.52 keV are confirmed qualitatively. The peaks of C and N elements are from the PANI, while peak of O element is due to water content which is not expelled from PANI electrode, as the electrode is not heated before characterisation. In the EDX spectrum of electrodes (A & B),

an additional peak of cobalt, of $Co(OH)_2$ is evidenced along with carbon, nitrogen and oxygen. The quantitative determination of the elements from EDX spectrum in terms of weight percentage and atomic percentage shows the formation of $Co(OH)_2$ in HNs (A & B). With increasing the cathodization time, the proportion of Co is increased and is more in HN of (B) than (A).

*3.3 Surface morphology*

The FESEM digital images of electrodes (A & B) are shown in Fig. 3; where $Co(OH)_2$ has been electrodeposited on highly porous well interconnected nanofiber network of PANI electrode for 5 and 15 minutes time at a constant voltage of -1.0V. With increasing the cathodization time, the amount of electrodeposited $Co(OH)_2$ mass is increased on the PANI electrode and in (A) electrode, the mass deposition of $Co(OH)_2$ is so least that, it cannot be observed in FESEM image. In the FESEM image (B), the mass deposited is as much as many nanofibers are in joined form.

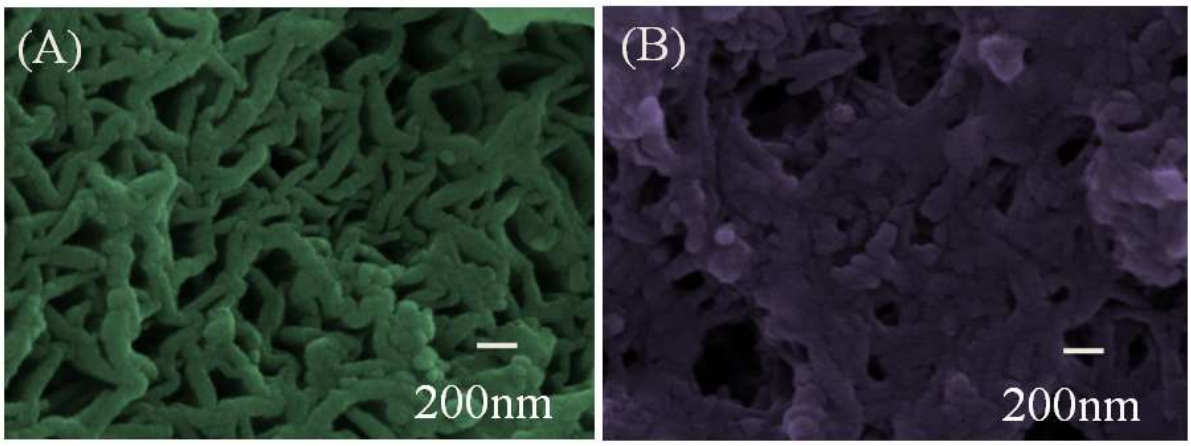


Fig. 3 The FESEM surface images of (A) and (B) electrode.

**4 Electrochemical measurements**

*4.1 CVs and electro-activity measurements*

All CVs are scanned in 1.0M NaOH electrolyte solution with a potential window of -0.2V- 0.5V for (A) & (B) *vs.* Ag/AgCl electrode at a scan rate of 10mV/s are as shown in Fig. 4. In both the electrodes, the current increases due to generation of electrons by oxidation of $Co(OH)_2$ which eventually drop a resistance at low potential and the current is not maintained and decreased on account of insufficient availability of electro-active sites for oxidation with scan rate of electrode from $Co(OH)_2$ to CoOOH. With increase in scan rate after first oxidation peak in vicinity of 0.3V potential, the current variations are minimised indicating decreased in resistance of electrode. After 0.35V, due to oxidation of CoOOH to $CoO_2$ increased in current with scan rate is observed. This indicates the variation of resistance with scan rate is one of indication of the pseudocapacitance. In the reverse CV, the reduction of materials is main cause for variation in current and hence in resistance. Thus, the presence of couple of redox peaks in the CV curves of HNs electrodes is attributed to the surface faradaic reaction at low potential as [20];

$$Co(OH)_2 + OH^- \leftrightarrow CoOOH + H_2O + e^-$$

While the faradaic reaction at higher potential can be presented as;

$$CoOOH + OH^{-} \leftrightarrow CoO_2 + H_2O + e^{-}$$

This indicates that the measured pseudocapacitance is mainly from the redox mechanism. The strong anodic peak at positive potential is due to the oxidation of $Co(OH)_2$ to CoOOH and the strong cathodic peak is for the reverse process. The weak anodic peak at positive potential is due to the oxidation of CoOOH to $CoO_2$, and the weak cathodic peak is for the reverse process.

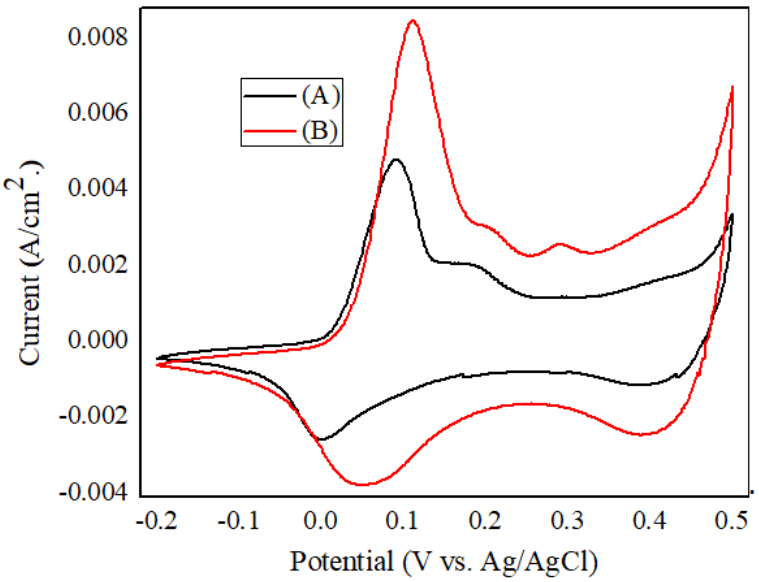


Fig. 4 CV curves at the scan rate of 10mV/s for (A & B) (-0.2V-0.5V) electrodes.

In this work, the SC values from CV are determined by calculating area of closed CV curve by

$$A = \int I(V)\mathrm{d}V \quad (1)$$

and charge '$q$' is obtained by

$$q = \frac{1}{v}\int I(V)dV \quad (2)$$

$$C_s = \frac{q}{m\nabla V} \quad (3)$$

$$E = \frac{1}{2}C_s(\nabla V)^2 \quad (4)$$

$$P = \frac{1}{2}C_s(\nabla V)\frac{dV}{dt} \quad (5)$$

where, $A$ is area of the closed CV curve (mW), $q$ is the charge density (mC/cm$^2$), $v = dV/dt$ is scan rate (mV/s), $Cs$ is specific capacitance (F/g), $m$ is mass of electrode materials (g), $\nabla V$ is the potential window of CV, $E$ is energy density (Wh/kg) and $P$ is power density (W/kg). The SC values obtained for (A) & (B) electrodes at 10mV/s are, 81.63F/g, and 142.8 F/g respectively. The values of charge density, energy density and power density are calculated by equation (2), (4) and (5) respectively and are shown in Table 1.

*4.2 Scan Rate Effect*

Moreover, Fig. 5 depicts the CV spectra of HN (A & B) electrodes obtained for different scan rates i.e. from 10 to 100 mV/s. In the present study, the voltage/potential across electrode increased by 10mV/s with successive increased in scan rate access more electro-active sites within same time is responsible for increase in current. Thus, the peak current values as well as currents at any instant are increased with respect

to scan rate to maintain approximately the same shape of CV for both electrodes. It is found that the anodic (oxidation) peaks shift to a more positive potential side, while cathodic (reduction) peaks shift to a more negative potential due to lag of current density at peak with increased scan rates. The peak current densities of both electrodes are increased with increasing scan rate. The nearly linear dependence of the current density on the scan rate reveals the reversible stability and fast response to oxidation/reduction, supporting for diffused limited process rather than surface limited [21]. Further, regarding the electrochemical capacitance trends with increasing current density with scan rate, the charge density and hence the SC and energy density of both electrodes is declined [Table 1]. This means that the current produced with increased in potential per second is not maintained. The retentions in (A) & (B) electrodes in charge density, SC and energy density are 60.8% & 67.8% respectively. At the same time, it is observed that the power density is increased with increase in scan rate and electrode (B) shows better performance of 85.2% retention in power density than electrode (A) as 83.5%.

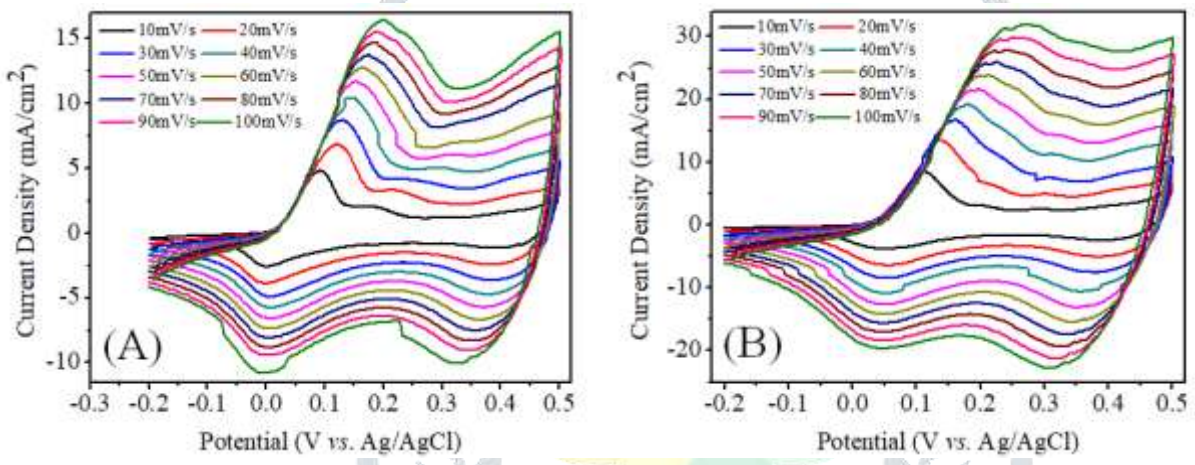


Fig. 5 Effect of scan rate on CV curves of (A) and (B) (-0.2 - 0.5V) electrodes in 1.0M NaOH electrolyte.

Table 1 Scan rate effect on the q, Cs, E and P values of (A) & (B) electrodes.

| Scan Rate/ Electr -odes | Physical Quantities | 10 | 20 | 30 | 40 | 50 | 60 | 70 | 80 | 90 | 100 | % of Reten -tion |
|---|---|---|---|---|---|---|---|---|---|---|---|---|
| (A) | q (mC/cm²) | 160 | 140 | 130 | 125 | 117.5 | 110.4 | 107.1 | 103.1 | 98.6 | 97.5 | 60.8% |
| | Cs (F/g) | 81.63 | 71.42 | 66.32 | 63.77 | 59.95 | 56.33 | 54.66 | 52.61 | 50.31 | 49.7 | |
| | E (Wh/kg) | 5.555 | 4.861 | 4.513 | 15.62 | 4.079 | 3.83 | 3.72 | 3.58 | 3.42 | 3.38 | |
| | P (W/kg) | 285.7 | 499.9 | 696.3 | 892.8 | 1049 | 1182 | 1339 | 1473 | 1584 | 1740 | 83.6% |
| (B) | q (mC/cm²) | 280 | 268.7 | 245.8 | 234.3 | 225 | 220.8 | 210.7 | 206.2 | 197.2 | 190 | 67.8% |
| | Cs (F/g) | 142.8 | 137.1 | 125.4 | 119.5 | 114.7 | 112.6 | 107.7 | 105.2 | 100.6 | 96.93 | |
| | E (Wh/kg) | 9.72 | 9.33 | 8.53 | 8.13 | 7.81 | 7.66 | 7.31 | 7.16 | 6.84 | 6.59 | |
| | P (W/kg) | 499.9 | 959.7 | 1316 | 1674 | 2008 | 2365 | 2634 | 2946 | 3169 | 3392 | 85.2% |

*4.3 Cyclic stability*

The cycling stabilities of the HN electrodes are depicted in Fig. 6 in 1.0M NaOH electrolyte at a scan rate of 40mV/s in the potential range of -0.2V to 0.5V for over 600 cycles for electrode (A) & 1000 cycles for electrode (B). The values of charge density, specific capacitance, energy density and power density are

decreased faster for electrode (A) than electrode (B) with increasing cycle number and the retention remained in above quantities are 39.49% and 82.98% respectively [Table 2]. The decrease of q, Cs, E and P with cycle number has same nature. The fading of charge density, specific capacitance and hence energy and power density are due to slight shifting of the oxidation peak of $Co(OH)_2$ to CoOOH towards CoOOH to $CoO_2$ peak, while the reduction $CoO_2$ to CoOOH peak is slight shifting towards CoOOH to $Co(OH)_2$ peak. The reduction peak CoOOH to $Co(OH)_2$ is disappeared for electrode (A) electrode after 600 cycles, indicating the slow oxidation of $Co^{2+}$ [$Co(OH)_2$] to $Co^{3+}$ [CoOOH]. In HNs $Co(OH)_2$ electrodes, the permanent conversion of $Co(OH)_2$ into $CoO_2$ is one of reason behind the decrease in q, Cs, E & P with cycle number of CV.

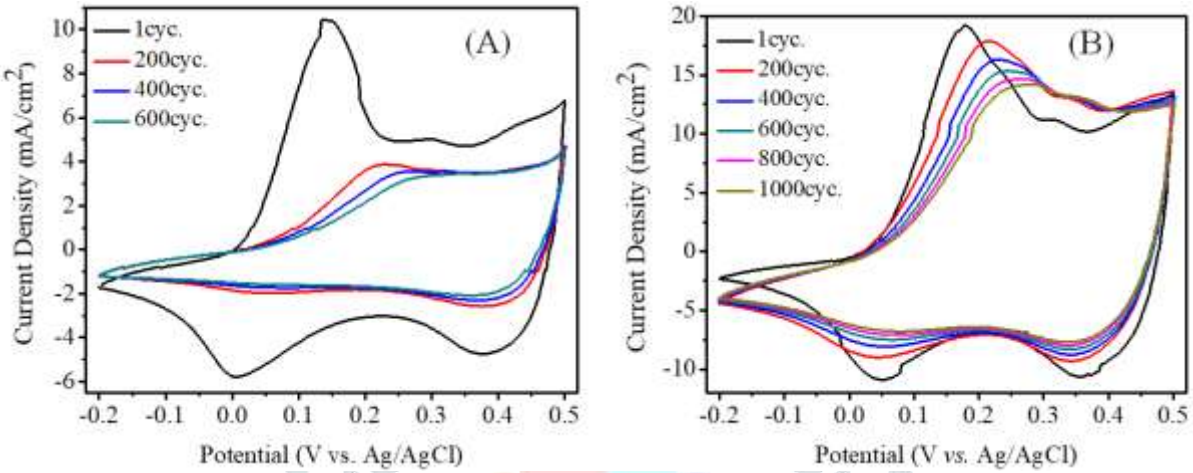


Fig. 6 CV stability curves of (A) and (B) electrodes.

Table 2: The relation between q, Cs, E and P values and cycle number for (A) & (B) electrodes.

| Cycle NO. /Electrodes | Physical Quantities | 1 | 200 | 400 | 600 | 800 | 1000 | % of Retention |
|---|---|---|---|---|---|---|---|---|
| (A) | q (mC/cm²) | 125 | 60 | 54.37 | 49.37 | --- | --- | 39.49% |
| | Cs (F/g) | 63.77 | 30.61 | 27.74 | 25.19 | --- | --- | |
| | E (Wh/kg) | 4.34 | 2.083 | 1.888 | 1.714 | --- | --- | |
| | P (W/kg) | 892.85 | 428.57 | 388.39 | 352.67 | --- | --- | |
| (B) | q (mC/cm²) | 234.37 | 232.12 | 219.5 | 210.1 | 202.0 | 194.5 | 82.98% |
| | Cs (F/g) | 119.57 | 118.43 | 112 | 107.2 | 103.06 | 99.23 | |
| | E (Wh/kg) | 8.138 | 8.059 | 7.621 | 7.296 | 7.013 | 6.753 | |
| | P (W/kg) | 1674.1 | 1658.0 | 1568 | 1500.8 | 1442.8 | 1389.2 | |

## Conclusion

Cobalt hydroxide ($Co(OH)_2$)-polyaniline hybrid nanocomposite electrodes, synthesized potentiostatically by electrochemical deposition method from an alkaline medium, demonstrate synergetic effect of supercapacitance with deposition time. Structural study has suggested amorphous nature of HNs electrodes. Morphological study indicates change in surface appearance. . The specific capacitance values of both electrodes are, 81.63F/g, and 142.8 F/g respectively, at a sweep rate of 10mV/s in 1.0M NaOH

electrolyte. The retention in charge density, specific capacitance, energy density and power density of HN electrodes are 39.49% and 82.98% respectively for the scan rate of 40mV/s.

**References**


1) M. Winter, R. Brodd, J. Chem. Rev., 104 (2004) 4245.
2) C. Largeot, C. Portet, J. Chmiola, P. Taberna, Y. Gogotsi, P. Simon, J. Am. Chem. Soc., 130 (2008) 2730.
3) L. L. Zhang, X. S. Zhao, Chem. Soc. Rev., 38 (2009) 2520.
4) P. Simon, Y. Gogotsi, Nat. Mater. 7 (2008) 845.
5) A. S. Arico, P. Bruce, B. Scrosati, J. M. Tarascon, W. van Schalkwijk, Nat. Mater., 4 (2005) 366.
6) G. Yu, L. Hu, M. Vosgueritchian, H. Wang, X. Xie, J. R. McDonough, X. Cui, Y. Cui, Z. Bao, Nano Lett., 11 (2011) 2905.
7) A. Buker, J. Power Sources, 91 (2000) 37.
8) D. Li, J. X. Huang, R. B. Kaner, Acc. Chem. Res., 42 (2009) 135.
9) S. Bhadra, D. Khastgir, N. K. Singha, J. H. Lee, Prog. Polym. Sci., 34 (2009) 783.
10) J. H. Park, O O. Park, J. Power Sources, 111 (2002) 185.
11) H. Zhou, Y. Lin, P. Yu, L. Su, L. Mao, Electrochem. Commun., 11 (2009) 965.
12) Y.Q. Dou, Y. Zhai, H. Liu, Y. Xia, B. Tu, D. Zhao, X. X. Liu, J. Power Sources, 196 (2011) 1608.
13) D. Yuan, T. Zhou, S. Zhou, W. Zou, S. Mo, N. Xia, Electrochem. Commun., 13 (2011) 242.
14) Z. Tai, X. Yan, Q. Xueb, J. Electrochem. Soc., 159 (2012) A1702.
15) A. Sumboja, C. Y. Foo, J. Yan, C. Yan, R. K. Gupta, P. S. Lee, J. Mater. Chem., 22 (2012) 23921.
16) Z. Chen, H. Lv, X. Zhu, D. Li, S. Zhang, X. Chen, Y. Song, J. Phys. Chem. C, 118 (2014) 27449.
17) W. F. Mak, G. Wee, V. Aravindan, N. Gupta, S. G. Mhaisalkar, S. Madhavia, J. Electrochem. Soc., 159 (2012) A1481.
18) X. Xia, Q. Hao, W. Lei, W. Wang, D. Sun, X. Wang, J. ***Mater. Chem.***, **22** (2012) 16844.
19) C. Polatides, G. Kyriacou, J. Appl. Electrochem., 35 (2005) 421.
20) V. Gupta, S. Gupta, N. Miura, J. Power Sources, 177 (2008) 685.
21) Y. G. Wang, H. Q. Li, Y. Y. Xia, Adv. Mater., 18 (2006) 2619.